Arch. Metall. Mater. **65** (2020), 3, 1189-1195

DOI: 10.24425/amm.2020.133238

M. BARA[1], J. DZIK[1], K. FELIKSIK[1], L. KOZIELSKI[1], B. WODECKA-DUŚ[1],
T. GORYCZKA[2], A. ZARYCKA[1], M. ADAMCZYK-HABRAJSKA[1*]

INFLUENCE OF CALCIUM IONS ON THE STRUCTURE AND PROPERTIES OF $LaMnO_3$

$La_{0,7}Ca_{0,3}MnO_3$ polycrystalline were synthesized from La_2O_3, CaO and MnO_2 powder mixture using a solid state reaction technique. The compound powders were obtained through the free sintering method at different temperatures and sintering times in order to study the influence of technological conditions on Ca doped La manganites. The most important physical features as structure, microstructure and morphology were described after X-ray diffraction investigation. Photographs of the specimen fractures were taken with SEM (scanning electron microscope) and they revealed high porosity of the tested material and great tendency for its grains to create agglomerates. Influence of doping and technological conditions on lattice parameters were studied by means of Rietveld analysis. The XRD measurements reveal that $La_{0,7}Ca_{0,3}MnO_3$ has orthorhombic symmetry with *Pnma* space group.

Keywords: LCMO, ceramics, manganites, X-ray diffraction, SEM.

1. Introduction

The manganese oxides of general formula $RE_{1-x}Y_xMnO_3$ (RE = rare earth, Y = Ca, Sr, Ba, Pb) have widespread application prospects due to their remarkable interrelated structural, magnetic and transport properties [1,2]. This coexistence of charge, orbital, lattice and magnetic degrees of freedom is strongly connected with the mixed valence (3^+-4^+) of the Mn ions [3]. Moreover, large part of the recent studies, both experimentally and theoretically [4,5] has been devoted to so-called CMR (colossal magnetoresistance) effects, which basics are not yet fully known.

Very recently, significant attention was paid to the manganese oxides as electrode materials for supercapacitors. Those storage devices are promising due to their high power density, fast charge/discharge process and long cycle life [6]. Good candidates for the fabrication of manganite-based supercapacitors devices are lanthanum magnanites (LMO). $LaMnO_3$ nanoparticles hybridized with $NiCo_2O_4$ on Ni foam delivers excellent cycling stability and are very efficient for the design of high-performance electrode materials in energy storage devices [7]. Moreover, $La_{0.85}Sr_{0.15}MnO_3$@$NiCo_2O_4$ electrode was designed for the first time with outstanding results of ultra-long cycle life, high power density and high efficiency [8].

Calcium-substituted lanthanum magnanites (LCMO) are also being investigated as an electrode for supercapacitors [9], but until now they have been especially studied as a potential high temperature solid oxide fuel cell cathodes (SOFC) [10]. For those manganites, several different synthesizing techniques have been reported, including solid-state reaction, which was used in this research. Calcium substitution is strictly responsible for double-exchange effect connected with mixed-valence of the Mn ions, and in addition, is responsible for both ferromagnetic coupling and charge transport. Furthermore, the material as a perovskite type is stable in the entire doping range ($0 > x > 1$), and its properties change simultaneously with the amount of Ca. For instance, LCMO is a ferromagnetic conductor in the range of $0.2 < x < 0.4$, while it also can be an antiferromagnetic insulator when the range comes closer to $x = 0$ or 1 [11]. Apart from magnetic properties, calcium substitution has a strong influence on structure, microstructure and morphology, and the study of this influence is the aim of this work.

The structure of LCMO ceramics is similar to that of the cubic perovskite. An important structural feature of the perovskite oxides is the oxygen octahedra. MnO octahedra can be easily distorted, both by changing amount of Ca and technological conditions [12]. The large sized La trivalent ions and Ca divalent ions occupy the A-site with 12-fold oxygen coordination.

[1] UNIVERSITY OF SILESIA, INSTITUTE OF MATERIALS ENGINEERING, FACULTY OF SCIENCE AND TECHNOLOGY, 12 ŻYTNIA STR., 41-200 SOSNOWIEC, POLAND
[2] UNIVERSITY OF SILESIA, INSTITUTE OF MATERIALS ENGINEERING, FACULTY OF SCIENCE AND TECHNOLOGY, 75 PUŁKU PIECHOTY 1A STR., 41-500 CHORZÓW, POLAND

* Corresponding author: malgorzata.adamczyk-habrajska@us.edu.pl

The smaller Mn ions (which are in the mixed-valence state) are located in the centre of an oxygen octahedron. For the stoichiometric oxide Mn ions proportions (states 3^+ and 4^+) are 1-x and x, respectively. As it was quoted before, perovskite-type features of LCMO and its MnO octahedra are determined with doping level $x = Mn^{4+}/(Mn^{3+} + Mn^{4+})$, and the average size of cations A (r_A), however a third relevant parameter, degree of disorder at site A $\sigma 2 = (r^2_A) - (r_A)^2$ is often taken into consideration [3,13]. The structure is governed by the tolerance factor *t*, and it is stable within the range of $0.75 \leq t \leq 1.00$. Perfect cubic structure is guaranteed with the tolerance factor of $t = 1$. An increase of the Calcium dopant reduces the tolerance factor and simultaneously lowers a symmetry from cubic to rhombohedral and farther, to orthorhombic structure [14]. Mefford et al. [15] introduced the anion charge storage mechanism in electrochemical reactions of the $LaMnO_3$ perovskite. This theory included oxygen vacancy intercalation and oxygen excess insertion mechanisms. It was the first example of anion-intercalation-type pseudocapacitance as well as the oxygen – vacancymediated redox has been applied firstly for fast energy storage [9,16].

2. Experimental

$La_{0,7}Ca_{0,3}MnO_3$ polycrystalline were synthesized using a solid state reaction technique. The starting materials were La_2O_3, CaO and MnO_2 oxides of the 'chem. pure' grade. Subsequently the required amounts of chemicals were derived from stoichiometric calculations on the basis of the general formula. All compounds were weighed and milled for 24 h, until they became homogeneous. Powder mixtures with appropriate molar ratio were pressed into 30 mm-diameter pellets under a pressure of 100 MPa. The synthesis of the material was conducted at 673 K for 1.5 h. The specimens were crushed, further milled, formed again to their final form into 10 mm-diameter pellets under a pressure of 600 MPa and sintered. The free sintering was obtained in FCF 4/150M chamber furnace. Three different series of samples differing in technological conditions were prepared (Table 1). First part (LCMO I) was sintered at 1473 K for 6 h in air, second (LCMO II) and third part (LCMO III) were sintered at 1573 K, for 12 h and 6 h in air, respectively. At the sintering, the aluminum oxide was used as a ballast. The samples were slow cooled in air (5 K/h). After the preparation process a significant decrease in the volume of all prepared samples was observed. In order to study the density and porosity, all samples were measured and weighed both before and after sintering.

TABLE 1

Synthesis and free sintering technological conditions for LCMO series I-III

Synthesis material	Series	Synthesis $T_{synt}\|t_{synt}\|dT/dt$	Free sintering $T_{fs}\|t_{fs}\|dT/dt$
$La_{0.7}Ca_{0.3}MnO_3$	**LCMO I**	673 K| 1.5 h |5 K/min	1473 K| 6 h |5 K/min
	LCMO II		1573 K| 12 h |5 K/min
	LCMO III		1573 K| 6 h |5 K/min

The morphology and chemical composition, including mapping of samples, were examined by scanning electron microscope in association with energy dispersive X-ray analysis SEM-EDAX (JEOL JSM-7100F TTL LV).

The phase identification of samples and their refined lattice parameters were carried out by XRD (X-ray diffractometer) in air with Cu K_α radiation (λ – 1,54178 Å) – Philips model X'Pert in association with Rietveld analysis. The scanning region and range was equal to $10° < 2\theta < 140°$ with a step of 0.05° and a counting time of 10 s/step. The phase identification was done using the ICDD PDF-4 database. The LHPM computer program, version 4.2, was used to calculate the lattice parameters.

3. Results and Discussion

The morphology is shown in Fig. 1. In order to reveal differences between series prepared in different technological conditions, the scanning electron micrographs were taken for each of the series. The micrographs were performed on the fractured surface of the ceramics at room temperature. Obtained micrographs revealed significant differences in shape and size of grains of samples sintered in different temperatures. Samples sintered at higher temperature have similar morphology and high tendency for grain growth – the higher the temperature, the bigger the grains, however grain boundaries fade away with the increase of the temperature. The surface of the fracture runs across the grains. All of the samples are characterized by high porosity and have high tendency to create agglomerates. The results fit well with hydrostatic measurements of relative density and porosity (Table 2) and additionally show strong influence of sintering temperature on those parameters. Even though higher temperature significantly lowers the porosity of the samples, this porosity still remains high, which is important when considering potential applications. Chosen values of time sintering do not affect any of the parameters.

Similar results were presented by B. Bruś et al. [17] for pure Lanthanum Manganites. The authors compare the samples prepared in different technological conditions, both sintering temperature and time. All of the samples are characterized by high porosity, which decreases with higher temperature. What is more, the authors prove that while sintering temperature and time increase, the grain size in pure LMO increases and the grains boundaries slowly fade away. The size of grains is comprised within the range of $0,8 > x > 1,2$ μm.

As a comparison, Calcium-substituted Lanthanum Manganite powders with x = 0.3 concentration were examined in work [18]. The authors additionally measured the particle size around 1 μm.

Qualitative analysis revealed the presence of chemicals that fit the assumed stoichiometric calculations, as well as the chemical composition in all samples. There are no impurity elements observed. The EDS data for all material groups are presented in Fig. 2. Quantitative analyses were performed for all samples (Table 3). All atomic percentage of chemical elements obtained

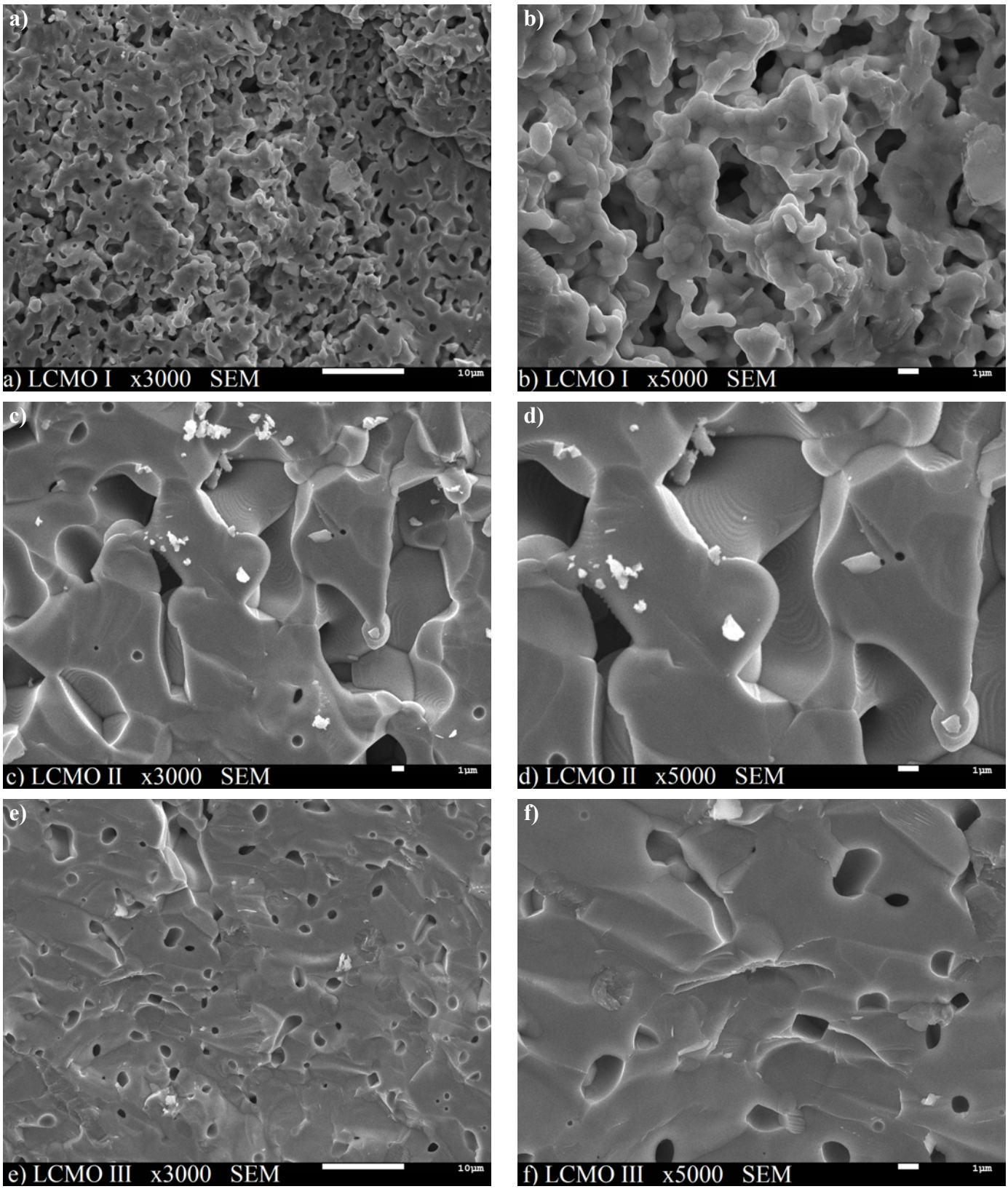

Fig. 1. SEM images of LCMO I (a, b), LCMO II (c, d), LCMO III (e, f) ceramics (3000× and 5000× magnification)

are close to theoretical. The results suggest, that applied sintering conditions favor the synthesis of LCMO material.

Elements distribution for series LCMO I-III is presented in the elemental mapping images (Fig. 3). The presence of each element is shown in the form of points, while density informs about the concentration. Obtained mapping reflects the homogeneous distribution of the constituent elements. Some places are characterized by less concentration, which is related to the microstructural features of the material like high porosity. Changing technological conditions does not affect the distribu-

TABLE 2

Hydrostatic measurements of LCMO I-III. Influence of technological conditions on relative density and porosity of the tested samples

Synthesis material	Series	Volume loss [%]	Density gained [%]	Relative density [g/cm^3]:	Porosity [%]
$La_{0.7}Ca_{0.3}MnO_3$	**LCMO I**	42,40	50,51	4,31	18,78
	LCMO II	51,30	78,72	4,65	5,40
	LCMO III	50,50	76,45	4,52	5,11

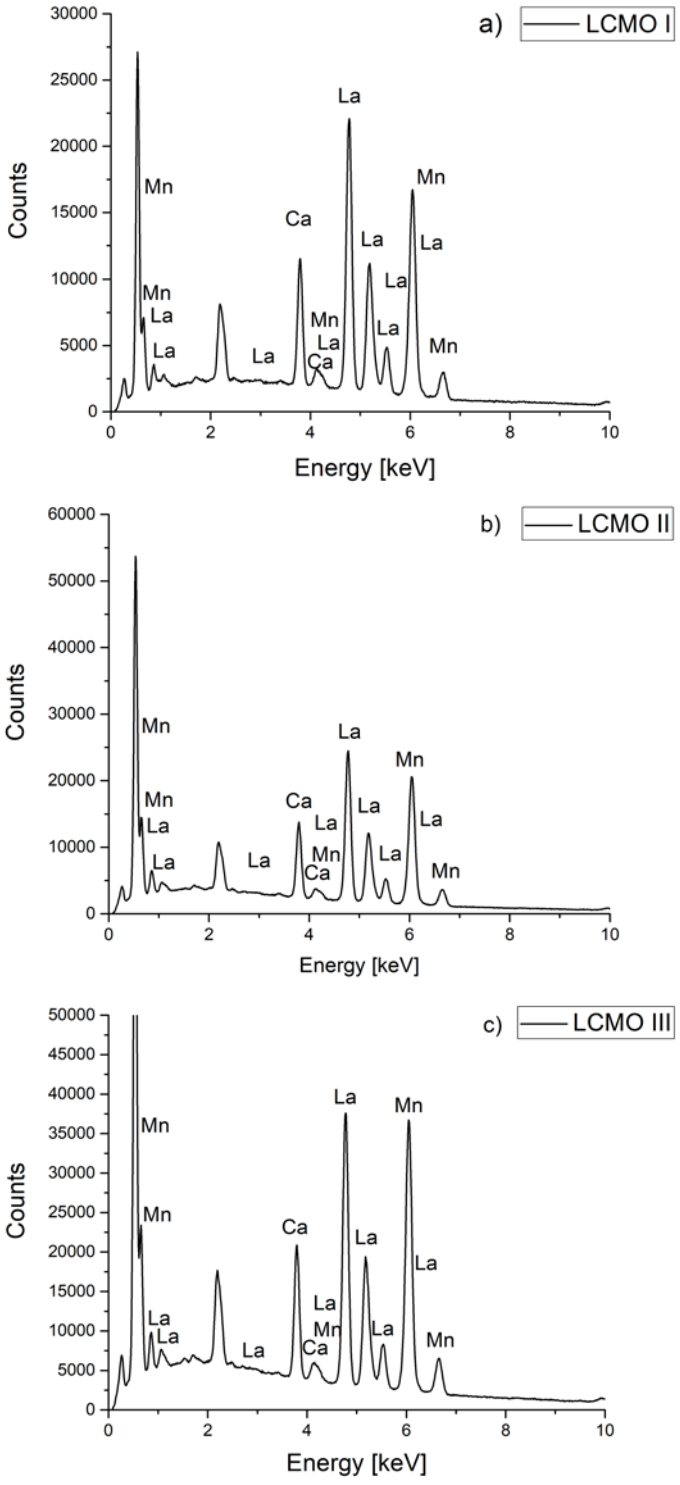

Fig. 2. EDS data obtained for LCMO I (a), LCMO II (b), LCMO III (c) ceramics

TABLE 3

Quantitative analyses performed for all material series

	Theoretical [at. %]	Experimental [at. %]		
	LCMO	LCMO I	LCMO II	LCMO III
La	33	39	37	34
Ca	17	13	13	13
Mn	50	48	50	53

tion of elements. In the work of S.P. Altintas et al. [19], the authors presented similar, homogeneous elements distribution for LCMO synthesized in the same preparation conditions but higher temperature 1623 K.

Structural analysis (Fig. 4) confirmed that all samples have orthorhombic structure with Pnma space group. The obtained diffraction reflections and calculated values of d_{hkl} fit in the values of the perovskite-type standard. Because of possible ceramic texturing occurring during forming the samples some small deviations in the position of diffraction lines and in the intensity may be seen. Phase analysis revealed that samples from both series I and II are single-phased, however on the spectra from series III few multi-phase areas may be seen, especially in the range of $20^o < 2\theta < 30^o$ and around 50^o, which is probably a result with larger than average conglomerates.

Elementary cell parameters a_0, b_0 and c_0 of samples sintered in all three technological conditions are presented in Table 4. Results were obtained by the Rietveld analysis and proved that as the sintering temperature increases, the volume of the elemental cell slightly decreases. What is worth to mention, the less vulnerable to technological conditions turned out to be factor c_0.

TABLE 4

Lattice parameters and cell volume of elementary LCMO ceramics

	Series	a_0 [nm]	b_0 [nm]	c_0 [nm]	$V \cdot 10^{-30}$ [m^3]
$La_{0.7}Ca_{0.3}MnO_3$	**LCMO I**	0,5458(9)	0,7700(4)	0,5479(1)	230,3
	LCMO II	0,5453(1)	0,7691(5)	0,5477(4)	229,7
	LCMO III	0,5456(4)	0,7692(8)	0,5476(8)	229,9

Comparing above results and research done by L. Rørmark et al. [20], it can be seen that changing technological conditions introduces the possibility to manipulate structure and lattice parameters, however more efficient is manipulating with dopant concentration. Basic structure of lanthanum manganites is rhombohedral, but adding just a small amount of Calcium dopant reduces the tolerance factor, deforms the perovskite and lowers the symmetry to orthorhombic. What is worth to mention, such effect is not easily received with other elements, like Strontium, where rhombohedral structure is maintained within a small amount of substitution.

Moreover, increasing the concentration of Calcium significantly decreases the size of cell volume, which is strictly connected to double-exchange effect and mixed-valence of the manganese ions. It is known that replacement of trivalent lanthanum ions with divalent calcium ions leads to the simultaneous

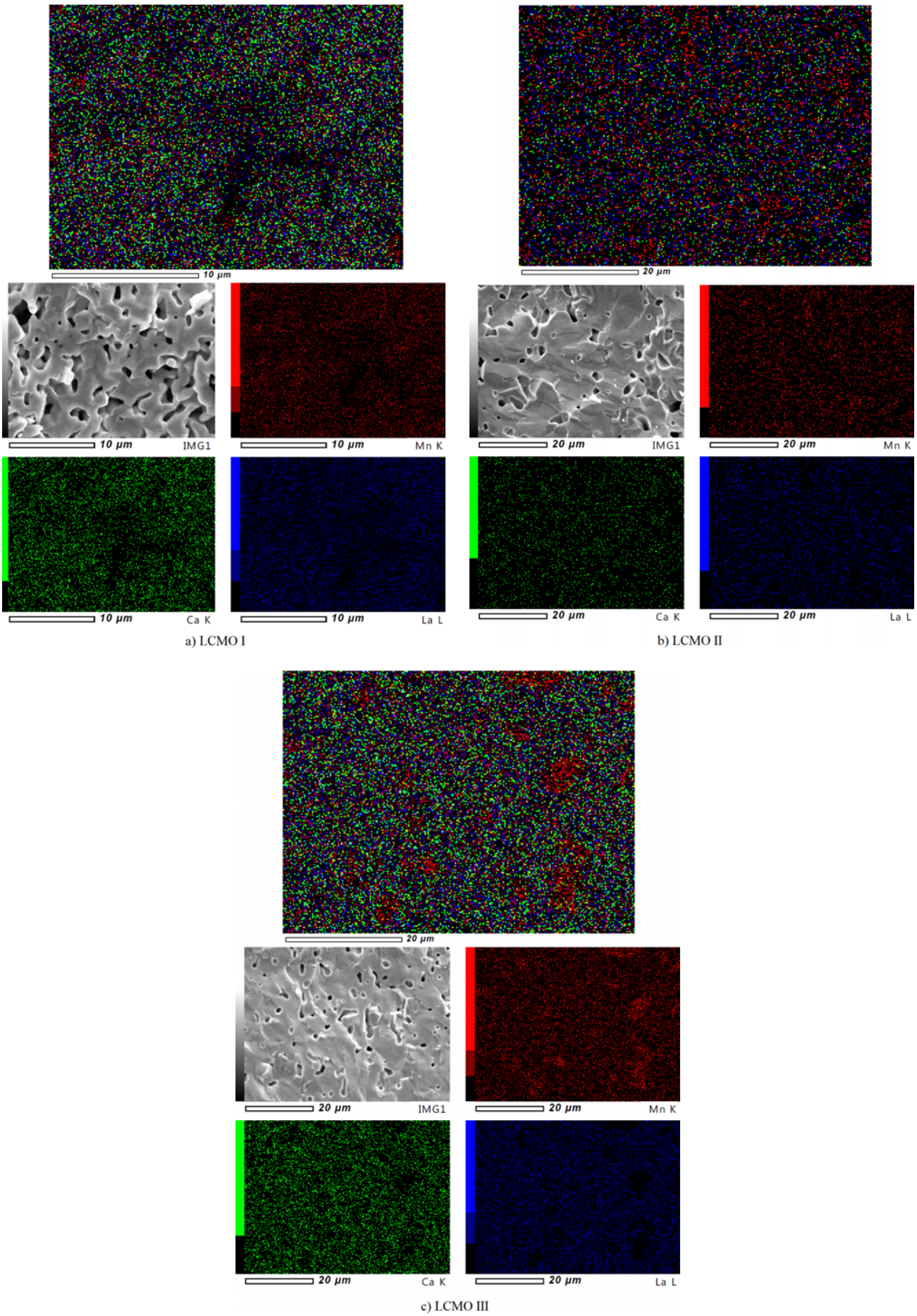

Fig. 3. Mapping images for LCMO I (a), LCMO II (b), LCMO III (c) ceramics

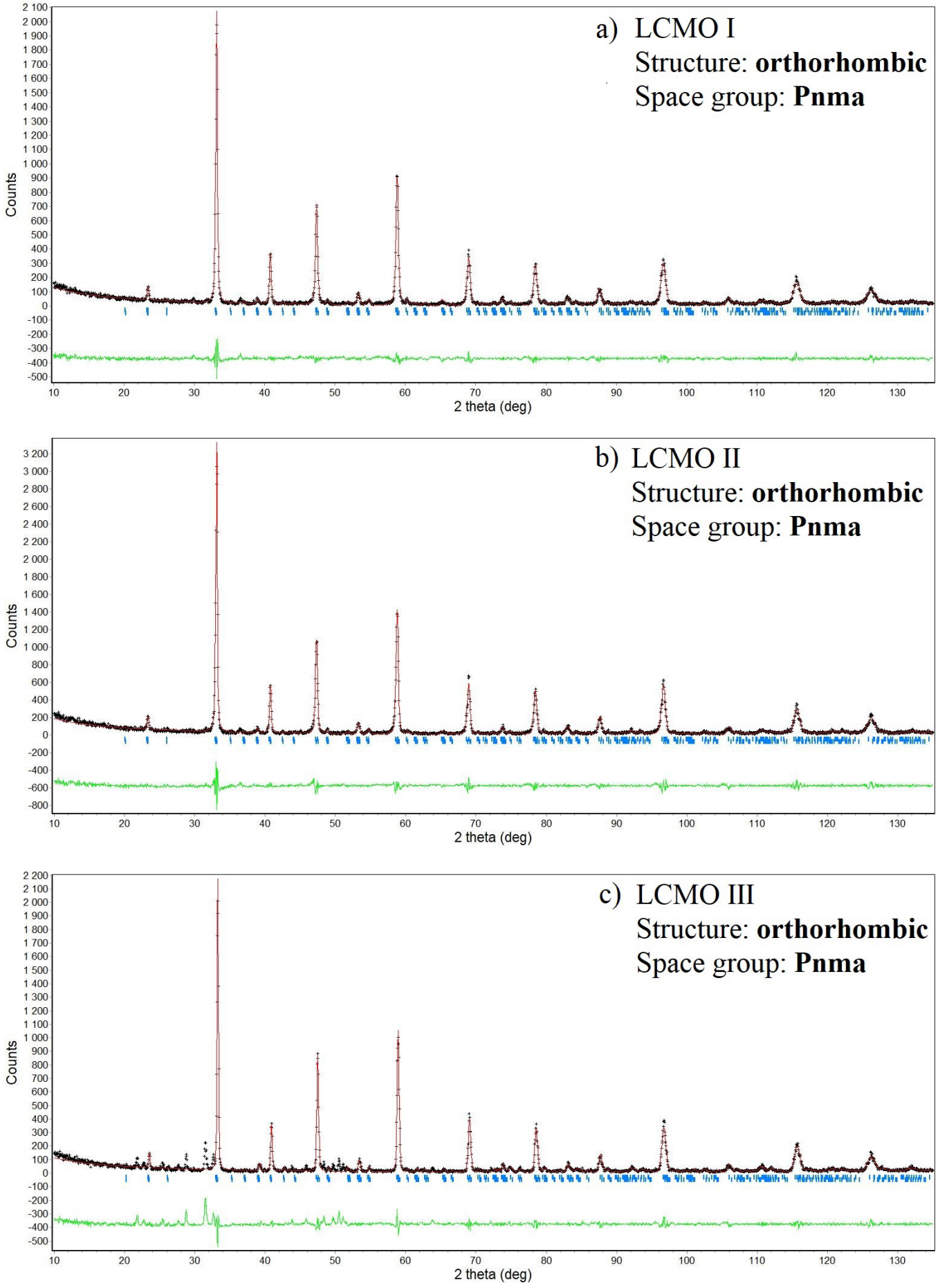

Fig. 4. X-ray diffraction patterns measured at room temperature for LCMO I (a), LCMO II (b), LCMO III (c)

occurrence of manganese ions in the form of Mn^{3+} and Mn^{4+}. Increasing the concentration of calcium increases the amount of Mn^{4+}, with smaller ionic radius r = 0.53 Å, decreases the amount of Mn^{3+} with ionic radii r = 0.65 Å, and consequently leads to the reduction in the size of cell volume.

4. Conclusions

$La_{0,7}Ca_{0,3}MnO_3$ polycrystalline were successfully synthesized via a solid state reaction technique with different time and temperature sintering. All discussed series of prepared materials were perovskite-type, characterized by orthorhombic structure with Pnma space group. The results suggest strong influence of chosen time sintering on physical and functional properties. Additionally, the EDS microanalysis confirmed the assumed stoichiometric, as well as the chemical composition in all samples. Comparing the obtained results to available literature it can be seen that the most influential on LCMO properties is the concentration of dopant. Changing the amount of Calcium changes the proportion between occurrence of Mn^{3+} and Mn^{4+} with different ionic radii, which determines the properties of the ceramics. The hydrostatic measurements and SEM analysis revealed high porosity of all tested materials, which alongside with great performance at operating in high temperatures is very precious for applications as a cathode in solid oxide fuel cells (SOFC).

REFERENCES

[1] C.N.R. Rao, A.K. Raychaudhuri, in: Colossal Magneto Resistance, Charge Ordering and Related Properties of Manganese Oxides, C.N.R. Rao, B. Raveau (Eds.), World Scientific, Singapore (1998).

[2] J.M.D. Coey, M. Viret, Adv. Phys. **48** (2), 167-293 (1999).

[3] A.-M. Haghiri-Gosnet, J.-P. Renard, J. Phys. D. Appl. Phys. **36**, 127-150 (2003).

[4] E. Dagotto, T. Hotta, A. Moreo, Phys. Rep. **344**, 1-153 (2001).

[5] Y. Tokura, Y. Tomioka, J. Magn. Magn. Mater. **200**, 1-23 (1999).

[6] H. Nan, X. Hu, H. Tian, Mat. Sci. Semicon. Proc. **94**, 35-50 (2019).

[7] H. Tian, X. Lang, H. Nan, P. An, W. Zhang, X. Hu, J. Zhang, Electrochim. Acta. **318**, 651-659 (2019).

[8] X. Lang, H. Zhang, X. Xue, C. Li, X. Sun, Z. Liu, H. Nan, X. Hu, H. Tian, J. Power. Sources. **402**, 213-220 (2018).

[9] H. Mo, H. Nan, X. Lang, S. Liu, L. Qiao, X. Hu, H. Tian, Ceram. Int. **44**, 9733-9741 (2018).

[10] S. Faaland, K.D. Knudsen, M.A. Einarsrud, L. Rørmark, R. Høier, T. Grande, J. Solid. State. Chem. **140**, 320-330 (1998).

[11] S. Satpathy, Z.S. Popović, F.R. Vukajlović, Phys. Rev. Lett. **76** (6), 960-963 (1996).

[12] D.P. Kozlenko, B.N. Savenko, J. Phys-Condens. Mat. **16**, 9031-9036 (2004).

[13] P.W. Iwanowski, Monokryształy i nanocząstki wybranych manganitów i kobaltytów – wytwarzanie oraz właściwości magnetyczne, Polska Akademia Nauk, Warszawa (2014).

[14] M.A. Peña, J.L.G. Fierro, Chem. Rev. **101** (7), 1981-2018 (2001).

[15] J.T. Mefford, W.G. Hardin, S. Dai et al., Nat. Mater **13**, 726-732 (2014)

[16] X. Lang, H. Mo, X. Hu, H. Tian, Dalton Trans. **46**, 13720 (2017)

[17] B. Bruś, A. Zarycka, Arch. Metall. Mater. **61** (2), 857-862 (2016).

[18] Q. Shu, J. Zhang, B. Yan, J. Liu, Mater. Res. Bull. **44**, 649-653 (2009).

[19] S.P. Altintas, N. Mahamdioua, A. Amira, C. Terzioglu, J. Magn. Magn. Mater. **368**, 111-115 (2014).

[20] L. Rørmark, S. Stølen, K. Wiik, T. Grande, J. Solid. State. Chem. **163**, 186-193 (2002).